The Astrophysical Journal Letters, 946:L25 (15pp), 2023 March 20 https://doi.org/10.3847/2041-8213/acbd50

Limit on Supernova Emission in the Brightest Gamma-Ray Burst, GRB 221009A

Manisha Shrestha[1], David J. Sand[1], Kate D. Alexander[1], K. Azalee Bostroem[1,27], Griffin Hosseinzadeh[1], Jeniveve Pearson[1], Mojgan Aghakhanloo[1], József Vinkó[2,3,4,5], Jennifer E. Andrews[6], Jacob E. Jencson[7], M. J. Lundquist[8], Samuel Wyatt[9], D. Andrew Howell[10,11], Curtis McCully[10,11], Estefania Padilla Gonzalez[10,11], Craig Pellegrino[10,11], Giacomo Terreran[10,11], Daichi Hiramatsu[12,13], Megan Newsome[10,11], Joseph Farah[10,11], Saurabh W. Jha[14], Nathan Smith[1], J. Craig Wheeler[4], Clara Martínez-Vázquez[6], Julio A. Carballo-Bello[15], Alex Drlica-Wagner[16,17,18], David J. James[19,20], Burçin Mutlu-Pakdil[21], Guy S. Stringfellow[22], Joanna D. Sakowska[23], Noelia E. D. Noël[23], Clécio R. Bom[24], and Kyler Kuehn[25,26]

[1] Steward Observatory, University of Arizona, 933 North Cherry Avenue, Tucson, AZ 85721-0065, USA; mshrestha1@arizona.edu
[2] Konkoly Observatory, CSFK, Konkoly-Thege M. út 15-17, Budapest, 1121, Hungary
[3] ELTE Eötvös Loránd University, Institute of Physics, Pázmány Péter sétány 1/A, Budapest, 1117 Hungary
[4] University of Texas at Austin, 1 University Station C1400, Austin, TX 78712-0259, USA
[5] Department of Experimental Physics, University of Szeged, Dóm tér 9, Szeged, 6720, Hungary
[6] Gemini Observatory, 670 North A'ohoku Place, Hilo, HI 96720-2700, USA
[7] Department of Physics and Astronomy, The Johns Hopkins University, 3400 North Charles Street, Baltimore, MD 21218, USA
[8] W.M. Keck Observatory, 65-1120 Māmalahoa Highway, Kamuela, HI 96743-8431, USA
[9] Department of Astronomy, University of Washington, 3910 15th Avenue NE, Seattle, WA 98195-0002, USA
[10] Las Cumbres Observatory, 6740 Cortona Drive, Suite 102, Goleta, CA 93117-5575, USA
[11] Department of Physics, University of California, Santa Barbara, CA 93106-9530, USA
[12] Center for Astrophysics | Harvard & Smithsonian, 60 Garden Street, Cambridge, MA 02138-1516, USA
[13] The NSF AI Institute for Artificial Intelligence and Fundamental Interactions, USA
[14] Department of Physics and Astronomy, Rutgers, the State University of New Jersey, 136 Frelinghuysen Road, Piscataway, NJ 08854-8019, USA
[15] Instituto de Alta Investigación, Sede Esmeralda, Universidad de Tarapacá, Av. Luis Emilio Recabarren 2477, Iquique, Chile
[16] Fermi National Accelerator Laboratory, P.O. Box 500, Batavia, IL 60510, USA
[17] Kavli Institute for Cosmological Physics, University of Chicago, Chicago, IL 60637, USA
[18] Department of Astronomy and Astrophysics, University of Chicago, Chicago, IL 60637, USA
[19] ASTRAVEO LLC, P.O. Box 1668, MA 01931, USA
[20] Applied Materials Inc., 35 Dory Road, Gloucester, MA 01930, USA
[21] Department of Physics and Astronomy, Dartmouth College, Hanover, NH 03755, USA
[22] Center for Astrophysics and Space Astronomy, University of Colorado Boulder, UCB 389, Boulder, CO 80309-0389 USA
[23] Department of Physics, University of Surrey, Guildford GU2 7XH, UK
[24] Centro Brasileiro de Pesquisas Físicas, Rua Dr. Xavier Sigaud 150, 22290-180 Rio de Janeiro, RJ, Brazil
[25] Lowell Observatory, 1400 W Mars Hill Road, Flagstaff, AZ 86001, USA
[26] Australian Astronomical Optics, Macquarie University, North Ryde, NSW 2113, Australia
Received 2023 February 7; revised 2023 February 17; accepted 2023 February 19; published 2023 March 28

Abstract

We present photometric and spectroscopic observations of the extraordinary gamma-ray burst (GRB) 221009A in search of an associated supernova. Some past GRBs have shown bumps in the optical light curve that coincide with the emergence of supernova spectral features, but we do not detect any significant light-curve features in GRB 221009A, nor do we detect any clear sign of supernova spectral features. Using two well-studied GRB-associated supernovae (SN 2013dx, $M_{r,\max} = -19.54$; SN 2016jca, $M_{r,\max} = -19.04$) at a similar redshift as GRB 221009A ($z = 0.151$), we modeled how the emergence of a supernova would affect the light curve. If we assume the GRB afterglow to decay at the same rate as the X-ray data, the combination of afterglow and a supernova component is fainter than the observed GRB brightness. For the case where we assume the best-fit power law to the optical data as the GRB afterglow component, a supernova contribution should have created a clear bump in the light curve, assuming only extinction from the Milky Way. If we assume a higher extinction of $E(B-V) = 1.74$ mag (as has been suggested elsewhere), the supernova contribution would have been hard to detect, with a limit on the associated supernova of $M_{r,\max} \approx -19.54$. We do not observe any clear supernova features in our spectra, which were taken around the time of expected maximum light. The lack of a bright supernova associated with GRB 221009A may indicate that the energy from the explosion is mostly concentrated in the jet, leaving a lower energy budget available for the supernova.

Unified Astronomy Thesaurus concepts: Gamma-ray bursts (629); Supernovae (1668); Type Ic supernovae (1730); Photometry (1234); Spectroscopy (1558)

1. Introduction

Long gamma-ray bursts (GRBs) are thought to be produced by the explosion of very massive stars (Woosley & Bloom 2006; Hjorth & Bloom 2012). These explosions produce relativistic jets where internal dissipation via synchrotron radiation creates prompt emission in gamma rays on timescales of seconds. Subsequently, the interaction of the jet ejecta with

[27] LSSTC Catalyst Fellow.

the ambient medium produces afterglow emission across the electromagnetic spectrum lasting hours to weeks. A few days to weeks after the explosion, an emerging supernova (SN) is often observed as an excess above the afterglow emission.

Long GRBs are often associated with type Ic-BL SNe. SNe of this type are core-collapse events where the progenitor star has lost a significant amount of its hydrogen (H) and helium (He) envelope (Filippenko 1997). There are competing, plausible progenitor scenarios for SN Ic-BL, including single Wolf–Rayet stars (Gaskell et al. 1986; Smartt 2009) or binary massive stars (Podsiadlowski et al. 1993; Nomoto et al. 1995), which can explain the stripping of the H and He envelope. However, to date, the progenitors of these SNe have not been definitively identified (see Smartt 2009 for a review). These SNe have high ejecta expansion velocities of order 15,000–30,000 km s^{-1} (Drout et al. 2011; Modjaz et al. 2011, 2016; Cano et al. 2017a), which lead to broad spectra features. Interestingly, only SNe of type Ic-BL have been observed in association with long GRBs; however, many SNe Ic-BL have been observed without a GRB component (Modjaz et al. 2020). The fraction of long GRBs that are accompanied by a SN is still debated. Rossi et al. (2022b) found that for over 1400 long GRBs discovered by Swift through 2022, only 40–50 of them have associated SNe identified via a bump in the optical light curve, and 28 have spectroscopic confirmation. Dado & Dar (2018) found that for low redshifts, the number of GRBs with associated SNe are comparable to GRBs without SNe.

However, where deep spectroscopic observations are possible (low z cases), there are only four GRBs with no associated SN: GRB 060505 (Fynbo et al. 2006), GRB 060614 (Della Valle et al. 2006; Fynbo et al. 2006; Gal-Yam et al. 2006), GRB 111005A (MichałowskI et al. 2018; Tanga et al. 2018), and GRB 211211A (Rastinejad et al. 2022; Troja et al. 2022), which instead showed potential kilonova emission. For GRBs without deep spectroscopic observations, the identification of an SN bump in the light curve based purely on photometry can be challenging and often depends sensitively on the assumptions made when modeling the GRB afterglow. For example, Melandri et al. (2022) presented the results of an SN connected to GRB190114C (the first GRB with detected TeV emission) using various facilities, including Hubble Space Telescope (HST). They find a large range in the probable luminosity of the associated SN 2019jrj, largely due to uncertainties in estimating the time of the GRB jet break. Their study shows that late-time photometry is critical for constraining the jet-break time, which in turn helps to constrain the energy of the SN explosion connected to the GRB.

The recent GRB 221009A (R.A. (J2000) = 19:13:03.50, decl. (J2000) = +19:46:24.23; Laskar et al. 2022), at a redshift of $z = 0.151$ (de Ugarte Postigo et al. 2022b; Castro-Tirado et al. 2022), provides a unique opportunity to explore GRB physics in detail. In contrast to many other nearby GRBs, which are often underluminous compared to more distant "cosmological" GRBs at $z > 1$ (Dainotti et al. 2022), GRB 221009A is the brightest GRB to ever be detected by the Fermi Gamma-ray Burst Monitor (GBM; Veres et al. 2022) and has generated broad community interest.

It is also one of a very small number of GRBs with detected very high energy emission, with reports of photon energy reaching 18 TeV by the LHAASO group (Huang et al. 2022) and 251 TeV by Carpet-2 (Dzhappuev et al. 2022). The detection of very energetic photons in the TeV range such as in the case of GRB 190114C (MAGIC Collaboration et al. 2019) and now GRB 221009A, challenges our understanding of GRB physics. There is no firm consensus on the production mechanisms of these very high-energy photons in the range of GeV to TeV (see further discussions in Balaji et al. 2023; Mirabal 2023). Atteia (2022) have predicted that the next event like GRB 221009A has a 10% probability of being observed in the next 50 yr.

There is an ongoing large follow-up campaign using various ground-based telescopes covering the entire electromagnetic spectrum for GRB 221009A. Here, we present an extensive search for SN emission in GRB 221009A, focusing on the optical bands. First, we present the observations in Section 2. Results from photometric and spectroscopic observations are provided in Section 3. Finally, we discuss the implications of these observations, along with concluding remarks, in Section 4. Throughout this paper, we use UTC date and time. We assume a Λ cold dark matter universe with $H_0 = 70\,\mathrm{km\,s^{-1}\,Mpc^{-1}}$, $\Omega_m = 0.286$, and $\Omega_\lambda = 0.714$ (Bennett et al. 2014). Presented uncertainties are at the 1σ confidence level.

The extinction toward GRB 221009A is high, as it is at a Galactic latitude of $b = 4.^{\circ}3$ and may also include a host component and/or a component associated with the local environment of the explosion. The assumed extinction value can affect interpretations of any underlying SN component of the GRB. We derive an $E(B-V) = 1.32 \pm 0.06$ mag, representing a Milky Way-only extinction scenario (using Schlafly & Finkbeiner 2011). We note that studies have shown the extinction values from the maps of Schlegel et al. (1998), which Schlafly & Finkbeiner (2011) is based on, are unreliable for areas near the Galactic plane (Popowski et al. 2003). Recently Kann et al. (2023) found that the value of the extinction can be lower than the value predicted from Schlafly & Finkbeiner (2011) using the method from Rowles & Froebrich (2009). From their analysis, Kann et al. (2023) concluded that the extinction toward the GRB 221009A is $0.709 < E(B-V) < 1.32$ mag.

However, Fulton et al. (2023) analyzed the optical data and calculated a spectral index. They found that even after correcting for the Galactic extinction from Schlafly & Finkbeiner (2011), the optical and X-ray data do not agree. In order to address the discrepancy, they calculated the additional extinction required. This additional extinction changes with time, and their quoted average is $A_v = 5.3$. One of the reasons for additional extinction was attributed to host galactic extinction.

For our analysis in this paper we consider two extinction values of $E(B-V) = 1.32 \pm 0.06$ mag and $E(B-V) = 1.74$ mag. Throughout the paper, we assume $R_v = 3.1$, which translates into $A_v = 4.1$ and $A_v = 5.4$, respectively. We chose the simple case of Galactic extinction from Schlafly & Finkbeiner (2011), which is an upper limit from the Kann et al. (2023) analysis. In order to account for additional host galactic extinction, we also use the higher value reported by Fulton et al. (2023). This range of extinction is important for the search for an associated SN as the higher extinction can hide the emerging SN features.

2. Observations and Data Reduction

Following the discovery of GRB 221009A (Figure 1), we started an extensive ground-based follow-up campaign with the aim of detecting the SN associated with the GRB. We augment this data set with public archival data from the HST and the

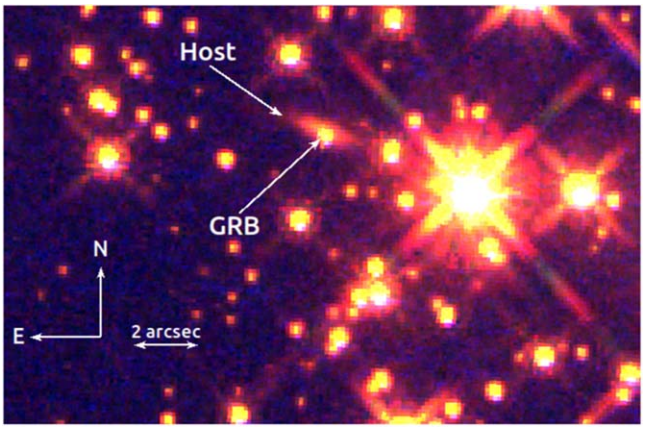

Figure 1. Combined HST images WFC3/UVIS and WFC3/IR (F625W, F125W, F160W) of the GRB 221009A field, observed on 2022 December 4. Note the clear appearance of an underlying host galaxy, with a disklike morphology. GRB 221009A is slightly offset from the center of the apparent host, off the disk plane.

results reported to the Gamma-Ray Burst Coordinates Network (GCN) service.

2.1. Photometry

In Figure 2 we present the photometric light curve of GRB 221009A from our own observations along with optical/near-infrared (NIR) data from GCN circulars and publicly available data from HST.

2.1.1. Ground-based Optical Observations

We performed optical photometric follow-up using the following instruments: the Multi-Object Double CCD Spectrographs/Imagers (MODS; Pogge et al. 2010) on the Large Binocular Telescope (LBT, 8.4 m twin telescope at Mt. Graham, Arizona); MuSCAT3 (Narita et al. 2020) on the Faulkes Telescope North (FTN, 2m telescope at Haleakalā Observatory, Hawaii; Brown et al. 2013)Global Supernova Project time; Binospec (Fabricant et al. 2019a) on the MMT (6.5 m telescope at Mt. Hopkins, Arizona); and the Goodman High-Throughput Spectrograph (GHTS; Clemens et al. 2004) on the Southern Astrophysical Research Telescope (SOAR, 4.1 m telescope at Cerro Pachón, Chile). Finally, GRB 221009A was observed by the Dark Energy Camera (DECam; Flaugher et al. 2015) instrument on the 4 m Blanco Telescope at CTIO as a target of opportunity as part of the DECam Local Volume Exploration (DELVE) survey (Drlica-Wagner et al. 2021, 2022). The details of the instruments and exposure times used, along with the observed magnitudes in different filters, are presented in Table 1.

Images from Las Cumbres Observatory and DECam were preprocessed using BANZAI (McCully et al. 2018) and the DECam Community Pipeline (Valdes & Gruendl 2014), respectively. We bias-subtracted and flat-fielded the remaining images using Python. We then performed aperture photometry using the Astropy Photutils package (Bradley et al. 2019) and calibrated to the Pan-STARRS1 catalog (Chambers et al. 2016). Table 1 and Figure 2 present all of our optical and NIR photometries.

2.1.2. HST Data

We obtained publicly available data from the Mikulski Archive for Space Telescopes on GRB 221009A taken with the Wide Field Camera 3 (WFC3; Dressel 2022) UVIS and IR channel on HST on three epochs, 2022 November 8, 2022 November 19, and 2022 December 4, and measured photometry on the calibrated and combined optical and NIR images (Program 17264, PI: A. J. Levan). In Table 2, we present our HST photometric results and other information. Photometry for the first epoch of HST data was also circulated via GCN by Levan et al. (2022); our measurements are in good agreement within the respective errors. We assume the HST filters F625W, F775W, F098M, F125W, and F160W correspond to r, i, y, J, and H filters, respectively. The results from our reductions are included in Figure 2. We note that the last two HST NIR data points could be contaminated due to the host galaxy.

2.1.3. GCN

We collected all optical and NIR data reported via the GCNs for GRB 221009A, and optical data are presented in Table 3. As we are looking for subtle changes in brightness, consistent filter throughputs and photometric systems are essential to this analysis. For this reason, we decided to only make use of data that have been reported in AB magnitudes and calibrated to the Pan-STARRS1 catalog (Chambers et al. 2016) for consistency. We corrected these data for Galactic extinction ($E(B-V)=1.32$ mag and $E(B-V)=1.74$ mag) before performing the data analysis.

2.2. Spectroscopy

We took our first optical spectrum of GRB 221009A 10.4 days after the Burst Alert Telescope (BAT) trigger with the 10 m Hobby–Eberly Telescope (HET; Ramsey et al. 1998; Shetrone et al. 2007; Hill et al. 2021) using the red arm of the Low-Resolution Spectrograph-2 (LRS2-R) having a $12'' \times 6''$ integral field unit and covering the 6450–8470 Å wavelength interval with a resolution of $R \sim 1800$ (Evans et al. 2016). Sky subtraction and wavelength and flux calibrations were performed by applying the Panacea[28] pipeline implemented at HET. Further details on the instrument configuration and the standard data reduction steps can be found in Yang et al. (2020).

Furthermore, we observed the location of GRB 221009A using the Binospec imaging spectrograph on the MMT (Fabricant et al. 2019a) for three different epochs. We used a long slit with a width of $1''$. For the observations done on 2022 October 25 (+15.48 days) and 2022 October 30 (+20.47 days), the 270 line mm^{-1} grating was used with central wavelengths of 6500 Å and 7500 Å, respectively, as presented in Table 4. For the 2022 October 27 (+17.49 days) observation, we used the 600 line mm^{-1} grating with a central wavelength of 7500 Å. We performed the initial data processing of flat-fielding, sky subtraction, and wavelength and flux calibrations using the Binospec Interface Description Language (IDL) pipeline (Kansky et al. 2019).[29] 1D spectra were extracted employing standard procedures using the Image Reduction and Analysis Facility (IRAF[30]). To account for slit losses, we scaled the spectrum to match the photometric data of GRB

[28] https://github.com/grzeimann/Panacea

[29] https://bitbucket.org/chil_sai/binospec/wiki/Home

[30] IRAF (Tody 1986, 1993) was distributed by the National Optical Astronomy Observatory, which was managed by the Association of Universities for Research in Astronomy (AURA) under a cooperative agreement with the National Science Foundation.

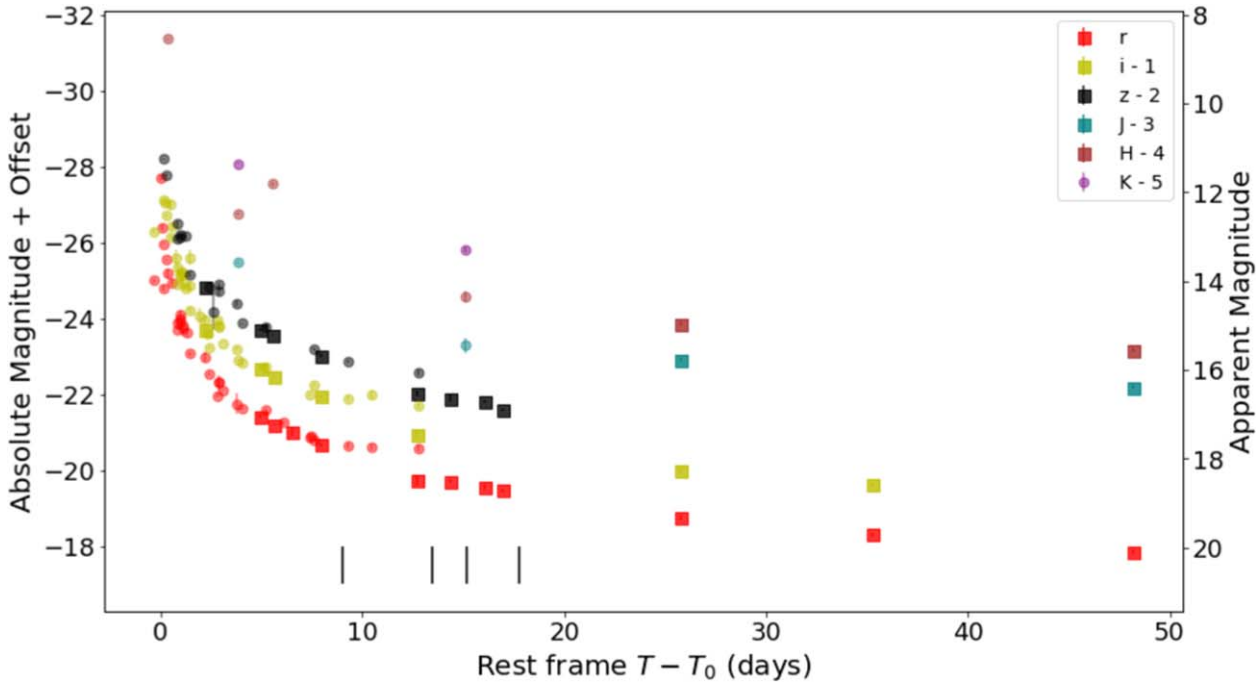

Figure 2. Optical light-curve data in r, i, z, J, H, K filters from GCN (circles) and data reduced by our group (squares). These values are from Tables 1, 2, and 3 and corrected for Galactic extinction. The vertical black lines correspond to the time of our spectral observations.

Table 1
GRB 221009A Ground-based Photometric Data

Date (UT)	MJD	Facility	Instrument	$t - t_0$ (days)	Exposure (s)	r (mag)	i (mag)	z (mag)	GCN
2022-10-12	59,864.11	LBT	MODS	2.5	6×120	⋯	19.00 ± 0.02	18.26 ± 0.01	32759[a]
2022-10-15	59,867.27	FTN	MuSCAT3	5.7	3×300	21.13 ± 0.06	20.05 ± 0.05	19.39 ± 0.05	32771[b]
2022-10-15	59,867.99	CTIO	DECam	6.4	1×180	21.34 ± 0.03	20.25 ± 0.02	19.52 ± 0.02	⋯
2022-10-17	59,869.03	SOAR	GHTS	7.4	3×180	21.53 ± 0.10	20.42 ± 0.10	19.75 ± 0.12	⋯
2022-10-18	59,870.75	FTN	MuSCAT3	9.2	3×300	21.88 ± 0.06	20.77 ± 0.04	20.06 ± 0.04	⋯
2022-10-24	59,876.20	FTN	MuSCAT3	14.6	3×300	22.82 ± 0.15	21.76 ± 0.10	21.07 ± 0.07	⋯
2022-10-26	59,878.10	MMT	Binospec	16.5	16×30	22.83 ± 0.07	⋯	21.19 ± 0.08	⋯
2022-10-28	59,880.07	MMT	Binospec	18.5	16×30	23.00 ± 0.07	⋯	21.29 ± 0.04	⋯
2022-10-29	59,881.07	MMT	Binospec	19.5	16×30	23.08 ± 0.06	⋯	21.50 ± 0.04	⋯

Notes. No correction for Galactic extinction has been applied.
[a] (Shresta et al. 2022).
[b] (Shrestha et al. 2022).

Table 2
HST Public Data of GRB 221009A

Date (UT)	MJD	$t - t_0$ (days)	Instrument	F625W	F775W	F098M	F125W	F160W
2022-11-8	59,891.27	29.68	WFC3	23.79 ± 0.32	22.72 ± 0.26	21.10 ± 0.08	20.49 ± 0.05	20.14 ± 0.05
2022-11-19	59,902.18	40.59	WFC3	24.24 ± 0.51	23.08 ± 0.40	⋯	⋯	⋯
2022-12-4	59,917.06	55.46	WFC3	24.70 ± 0.38	⋯	21.82 ± 0.11	21.21 ± 0.07	20.83 ± 0.07

Note. No correction for Galactic extinction has been applied. The F625W and F775W filters are from WFC3/UVIS, while the F098M, F125W, and F160W filters are from WFC3/IR.

221009A using a Python routine from Hosseinzadeh & Gomez (2022). Finally, we corrected the spectrum for Galactic extinction using the Python `extinction` package (Barbary 2016).

A log of our spectroscopic observations can be seen in Table 4, and the spectra can be seen in Figure 7 after correction for extinction and subtraction of an afterglow component as discussed in Section 3.2.

Table 3
GCN Photometric Data of GRB 221009A

GCN	Telescope	$t - t_0$ (days)	r (mag)	i (mag)	z (mag)	J (mag)	H (mag)	K (mag)	References
32647	NEXT	0.0087	14.93 ± 0.05	⋯	⋯	⋯	⋯	⋯	Xu et al. (2022)
32645	AZT-33IK	0.01223	14.84 ± 0.09	⋯	⋯	⋯	⋯	⋯	Belkin et al. (2022c)
32662	GIT	0.094	16.16 ± 0.07	⋯	⋯	⋯	⋯	⋯	Kumar et al. (2022)
32646	MeerLICHT	0.17	17.76 ± 0.08	15.58 ± 0.03	14.89 ± 0.03	⋯	⋯	⋯	de Wet et al. (2022)
32644	BOOTES-2/ TELMA	0.19	16.57 ± 0.02	⋯	⋯	⋯	⋯	⋯	Hu et al. (2022)
32638	LT	0.29	17.00 ± 0.03	15.98 ± 0.03	15.32 ± 0.03	⋯	⋯	⋯	Perley (2022)
32755	REM	0.4	⋯	⋯	⋯	⋯	12.62 ± 0.02	⋯	D'Avanzo et al. (2022)
32652	REM	0.434	17.36 ± 0.12	⋯	⋯	⋯	⋯	⋯	Brivio et al. (2022)
32664	CDK	0.54	⋯	15.70 ± 0.13	⋯	⋯	⋯	⋯	Romanov (2022a)
32659	LOAO	0.63	17.55 ± 0.06	16.41 ± 0.05	⋯	⋯	⋯	⋯	Paek et al. (2022)
32669	Nickel	0.65	17.6 ± 0.1	16.3 ± 0.1	⋯	⋯	⋯	⋯	Vidal et al. (2022)
32730	Mitsume	0.9320	⋯	17.1 ± 0.2	⋯	⋯	⋯	⋯	Sasada et al. (2022)
32729	AZT-33IK	1.02	18.84 ± 0.02	17.8 ± 0.02	16.99 ± 0.02	⋯	⋯	⋯	Zaznobin et al. (2022)
32667	SLT-40 cm	1.04	18.67 ± 0.16	17.38 ± 0.09	16.60 ± 0.09	⋯	⋯	⋯	Chen et al. (2022)
32795	GRANDMA	1.1360	18.57 ± 0.05	17.56 ± 0.05	16.93 ± 0.05	⋯	⋯	⋯	Rajabov et al. (2022)
32684	Sintez-Newton	1.163	18.43 ± 0.10	⋯	⋯	⋯	⋯	⋯	Belkin et al. (2022b)
32670	AZT-20	1.164	18.64 ± 0.03	17.58 ± 0.01	16.87 ± 0.05	⋯	⋯	⋯	Kim et al. (2022)
32693	Las Cumbres 1 m	1.22	18.80 ± 0.21	17.8 ± 0.2	⋯	⋯	⋯	⋯	Strausbaugh & Cucchiara (2022a)
32709	RC80	1.26	18.74 ± 0.12	17.5 ± 0.08	⋯	⋯	⋯	⋯	Vinko et al. (2022)
32678	BG3-Opal	1.48	⋯	17.92 ± 0.06	16.92 ± 0.05	⋯	⋯	⋯	Groot et al. (2022)
32679	T24 iTelescope	1.66	⋯	17.1 ± 0.2	⋯	⋯	⋯	⋯	Romanov (2022b)
32705	COATLI	2.63	⋯	19.10 ± 0.02	⋯	⋯	⋯	⋯	Butler et al. (2022)
33038	FTN	2.73	20.01 ± 0.03	19.48 ± 0.03	18.26 ± 0.01	⋯	⋯	⋯	Kimura et al. (2022)
32727	GMG	3.0	⋯	⋯	18.9	⋯	⋯	⋯	Mao et al. (2022)
32753	T120cm	3.25	20.23 ± 0.09	18.91 ± 0.11	18.35 ± 0.13	⋯	⋯	⋯	Schneider et al. (2022)
32743	RTT-150	3.3	20.24 ± 0.19	18.92 ± 0.04	18.10 ± 0.04	⋯	⋯	⋯	Bikmaev et al. (2022a)
32738	Las Cumbres 1 m	3.53	>21	>20.5	⋯	⋯	⋯	⋯	Strausbaugh & Cucchiara (2022b)
32739	LDT	3.57	20.44 ± 0.02	19.37 ± 0.01		⋯	⋯	⋯	O'Connor et al. (2022a)
32752	RTT-150	4.3	20.86 ± 0.27	19.50 ± 0.07	18.70 ± 0.06	⋯	⋯	⋯	Bikmaev et al. (2022b)
32750	Gemini	4.4	⋯	⋯	⋯	17.93 ± 0.03	17.23 ± 0.05	16.69 ± 0.02	O'Connor et al. (2022c)
32749	Gemini	4.437	⋯	19.8	⋯	⋯	⋯	⋯	Rastinejad & Fong (2022)
32758	Pan-STARRS1	4.67	20.92 ± 0.05	19.88 ± 0.02	19.21 ± 0.02	⋯	⋯	⋯	Huber et al. (2022)
32769	AZT-20	6.05	20.96 ± 0.05	20.00 ± 0.04	19.31 ± 0.08	⋯	⋯	⋯	Belkin et al. (2022a)
32804	TNG	7.3	⋯	⋯	⋯	⋯	16.45 ± 0.04	⋯	Ferro et al. (2022)
32809	LBT	8.58	21.63 ± 0.02	⋯	⋯	⋯	⋯	⋯	Rossi et al. (2022a)
32799	LDT	9.5	21.68 ± 0.07	20.72 ± 0.05	⋯	⋯	⋯	⋯	O'Connor et al. (2022b)
32818	AZT-20	12.05	21.94 ± 0.07	20.72 ± 0.11	⋯	⋯	⋯	⋯	Belkin et al. (2022c)
32860	Gemini	17.4	⋯	⋯	⋯	20.1 ± 0.2	19.43 ± 0.15	18.94 ± 0.08	O'Connor et al. (2022d)
32921	HST	29.68	23.61 ± 0.04	22.43 ± 0.04	⋯	⋯	⋯	⋯	Levan et al. (2022)

Note. No correction for Galactic extinction has been applied.

3. Supernova Limits

The observation of SN 1998bw coincident spatially and temporally with GRB 980425 (Galama et al. 1998; Iwamoto et al. 1998; Kulkarni et al. 1998) was the first direct evidence of the GRB–SN association. For nearby ($z < 0.3$) long GRBs, such as GRB 221009A, there have been observations of an associated SN (Hjorth & Bloom 2012) in all except four cases: GRB 060505 (Fynbo et al. 2006), GRB 060614 (Della Valle et al. 2006; Fynbo et al. 2006; Gal-Yam et al. 2006), GRB 111005A (MichałowskI et al. 2018; Tanga et al. 2018), and GRB 211211A (Rastinejad et al. 2022; Troja et al. 2022). However, the true fraction of long GRBs without an SN is unknown (Hjorth & Bloom 2012). The study of associated SNe

Table 4
Spectroscopic Observations

UT Date	MJD	Facility	Instrument	Filter	Grating	$t - t_0$ (days)	Exposure (s)
2022-10-21	59,873.10	HET	LRS2-R	⋯	VPH-Grism	10.40	1×2000
2022-10-25	59,877.07	MMT	Binospec	LP3800	270	15.48	4×1200
2022-10-27	59,879.08	MMT	Binospec	LP3800	600	17.49	5×1200
2022-10-30	59,882.06	MMT	Binospec	LP3800	270	20.47	4×1200

provides an important clue to the understanding of the progenitors and environment of these long GRBs. Thus, we search for SN signatures in our GRB 221009A light curves and spectra in Sections 3.1 and 3.2, respectively.

3.1. Light-curve Analysis

For our light-curve analysis, we focused on the *r* and *i* bands because we have better data coverage in these bands compared to the *z* band. The emission observed at the GRB position will have contributions from three potential components: the GRB afterglow, the SN, and the host galaxy. The host galaxy is detected in the WFC3/IR filters, whereas in the WFC3/UVIS filters, it is not clearly visible as shown in Figure 1. Therefore we do not explicitly model its contribution for our optical analysis. In addition, Levan et al. (2023) recently presented a detailed analysis of the GRB host galaxy, and they found the host extinction to be $A_V = 0.019^{+0.030}_{-0.014}$, which points to low host galaxy extinction, at least in some analyses. That said, we do consider two extinction scenarios as discussed earlier, with one focused solely on Milky Way extinction ($E(B-V) = 1.32$) and another which may include a host galaxy contribution ($E(B-V) = 1.74$; Fulton et al. 2023). We approached the search for the associated SN component using two different techniques.

For the first technique, we model the GRB optical afterglow using a broken power-law model, assuming the decay index from the X-Ray Telescope (XRT) data to avoid possible SN contamination in the optical data (e.g., Toy et al. 2016; Fulton et al. 2023). The reduced χ^2 for a one-break fit of the XRT data is 1.33, whereas for four breaks (the best-fit model) is 1.24. We also calculated the Bayesian information criterion: $\mathrm{BIC} = k\ln(n) - 2\ln(L)$ (Kass & Raftery 1995), where k is the number of fit parameter, n is the number of data points, and L is the estimation of the likelihood at its maximum. We find the ratio of BIC for the four-break model to one-break model to be 9.9, which shows that there is strong evidence against the higher-break model (Kass & Raftery 1995). Hence, we do not find a significant improvement in the fit beyond one break and thus use a one-break model for the remainder of the analysis. The one-break fit of the XRT data has a decay index of $\alpha_1 = 1.515 \pm 0.003$ before the break time of 0.6 days, and after the break, the decay index is $\alpha_2 = 1.663 \pm 0.006$[31] (Evans et al. 2009). The solid purple line represents this decay index in Figures 3 and 4. Hence, we force the decay index after 0.6 days for optical data to be 1.663 ± 0.006, which is the α_2 and is labeled "XRT BPL" in Figures 3 and 4.

We also fit all the optical data points with an empirical broken power law, whose best-fit is represented by the solid red and yellow lines for the *r* and *i* filters, respectively. The best-fit model to the optical data gives the decay index values of 0.64 before and 1.44 after the break time of 0.6 day for the *r*-band data. For the *i*-band data, the best-fit model has decay index values of 0.81 before and 1.46 after the break time of 0.6 days. These broken power-law fits to the optical data are labeled "GRB BPL" in Figures 3 and 4. In addition, we also fit a broken power law to limited data points in the *z* band, which are not shown here. The best fit gives decay indices of 0.97 and 1.38 before and after the break time of 0.6 days, respectively, which is consistent with *r*- and *i*-band data.

In addition to the power-law fits above, we consider an additional SN component using data directly from two SNe associated with GRBs: SN 2013dx/GRB 130702A (Toy et al. 2016) and SN 2016jca/GRB 161219b (Cano et al. 2017b). SN 2013dx ($M_{r,\max} = -19.54$) is at a redshift of 0.145, and SN 2016jca ($M_{r,\max} = -19.04$) is at a redshift of 0.1475, both of which are similar to the redshift of GRB 221009A; these objects were specially chosen so that we could do direct filter comparisons between them and GRB 221009A without any *K* correction. These comparisons in the *r* and *i* bands are presented in Figures 3 and 4, respectively. Each row in this figure represents a model for one SN, where the black solid line is the SN light curve. We note that Mazzali et al. (2021) and Ashall et al. (2019) have also carried out analysis of SN 2013dx and SN 2016jca, respectively. From their analysis they found the luminosities to be different from the models we considered in our analysis.

In order to determine the effect of the SN on the light curve of GRB 221009A qualitatively, we combined the afterglow component (purple solid line) with the SN component (black solid line). The resulting light curve is shown as a dashed line in the plot. For the case with a lower extinction value (left panels of Figures 3 and 4), the dashed lines initially underpredict the flux compared to the observed flux. This can be also seen in the residual plots shown in the bottom panels. During the SN peak, the match to the observed data is better. However, in the *r* band we find an excess in observed flux compared to the X-ray power law + SN model. For the case of $E(B-V) = 1.74$ mag, the dashed lines underpredict the flux compared to observed data at all times. The residual plots for all the cases show that the broken power law fitted to optical data produces the least residual, without any need for an SN component.

For the second method, we assume that the optical light curve is dominated by the GRB afterglow, and it is defined by the broken power-law fit to the optical data. As seen in the earlier discussion, this gives the least residual. In addition, the optical decay index in the *r* band after the break is $\alpha_{\mathrm{opt},r} = 1.44$ and for the *i* band is $\alpha_{\mathrm{opt},i} = 1.46$. The decay index for XRT is $\alpha_X = 1.663$. We see that the difference between the optical and X-ray decay indices is close to 1/4, which is expected for the slow cooling regime for the constant interstellar medium for the case where the synchrotron cooling break is between the optical

[31] https://www.swift.ac.uk/xrt_live_cat/01126853/

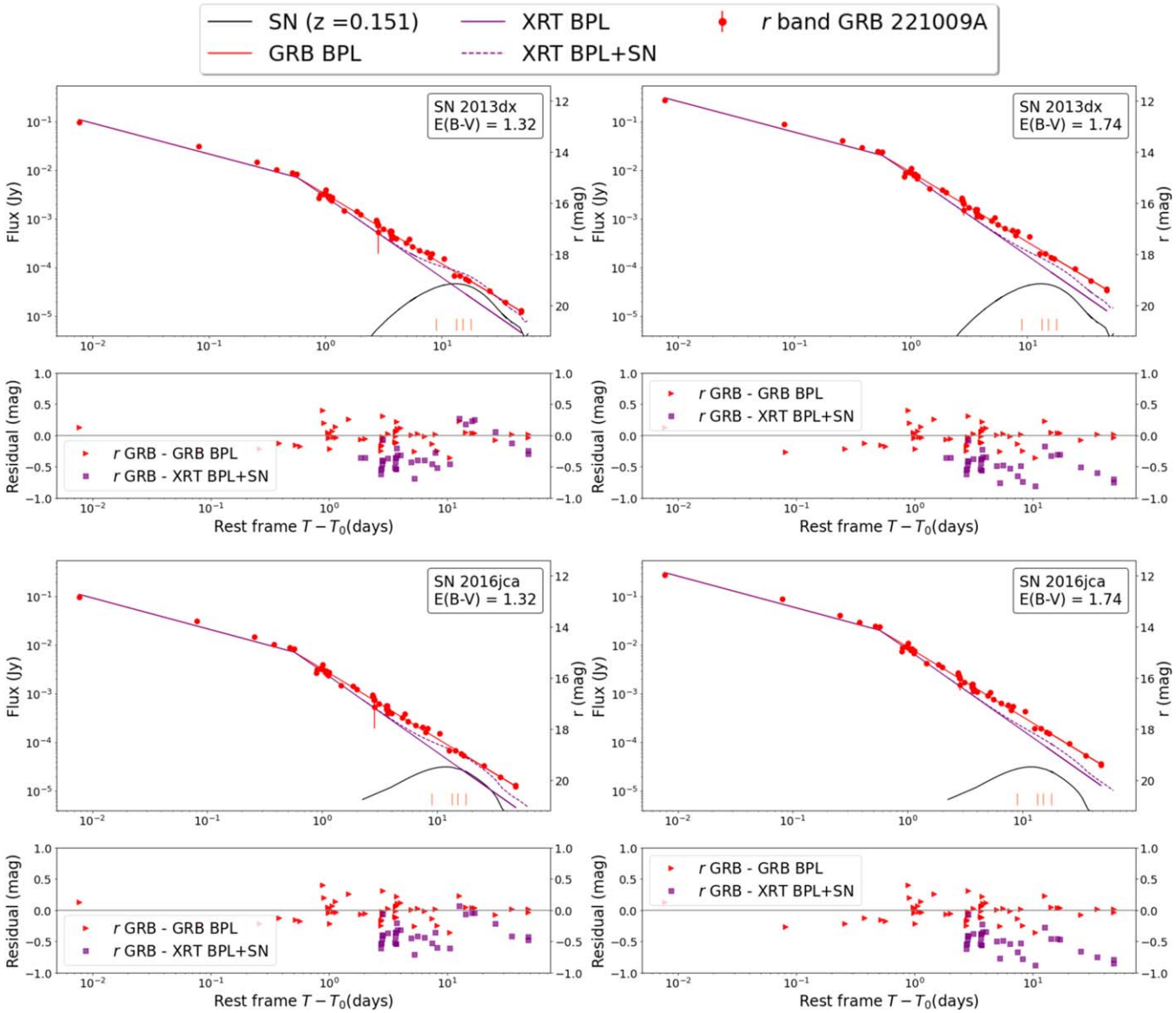

Figure 3. Light curves for the r filter for two different extinction values of $E(B-V) = 1.32$ mag (left column) and $E(B-V) = 1.74$ mag (right column) with a broken power-law fit to the data. Light-curve models of SN 2013dx (top row) and SN 2016jca (bottom row) are included as black solid lines along with GRB data. For each case, a residual plot in magnitude is presented. The purple squares are the difference between SN contribution plus GRB afterglow estimated by the XRT decay index and broken power-law estimate. The red triangles are the difference between the observed GRB magnitude and broken power-law estimate. The orange lines in the figure are the epochs for which we have spectroscopic observations. The residual plot shows that the SN component is not necessary to explain the light curve.

and the X-ray bands (Zaninoni et al. 2013). Laskar et al. (2023) show that an afterglow model with a wind-like density profile can also match the optical and X-ray light curves without the addition of an SN component. In their model, the cooling break is above the X-ray band, and the characteristic synchrotron frequency (corresponding to the minimum electron energy) is just below the optical band, which causes the optical light curves to decline more slowly than the X-rays. With this assumption, we investigated the effect of an associated SN in the light curve. We add the contribution of SN 2013dx and SN 2016jca to the GRB afterglow model with broken power law and decay index of 1.44 and 1.46 after the break for the r and i bands, respectively. For the case of $E(B-V) = 1.32$ mag, we see that both in the r (Figure 5) and i (Figure 6) bands, an SN bump would have been clear for both the SNe cases. However, if the $E(B-V)$ is high as 1.74 mag, then the bump is not clear in the light curves, and it could be hidden by the afterglow. This gives us a qualitative limit of $M_{r,\max} \approx -19.5$ mag.

3.2. Spectroscopic Analysis

We observed the location of GRB 221009A spectroscopically using the HET and MMT. The observations were taken at four different epochs to detect the broad spectral features, which are observed in type SNe Ic-BL associated with GRBs. In Figure 7, we present the results of spectroscopic observations done at the location of GRB 221009A on four different epochs using HET and MMT after smoothing. The spectra have been corrected for two different extinction values of $E(B-V) = 1.32$ mag (left panel) and $E(B-V) = 1.74$ mag (right panel). We note tentative, narrow Hα emission at $z = 0.151$ in the $+17.8$ days spectrum, which may also be visible in the $+10.4$ day HET spectrum as seen by Izzo et al.

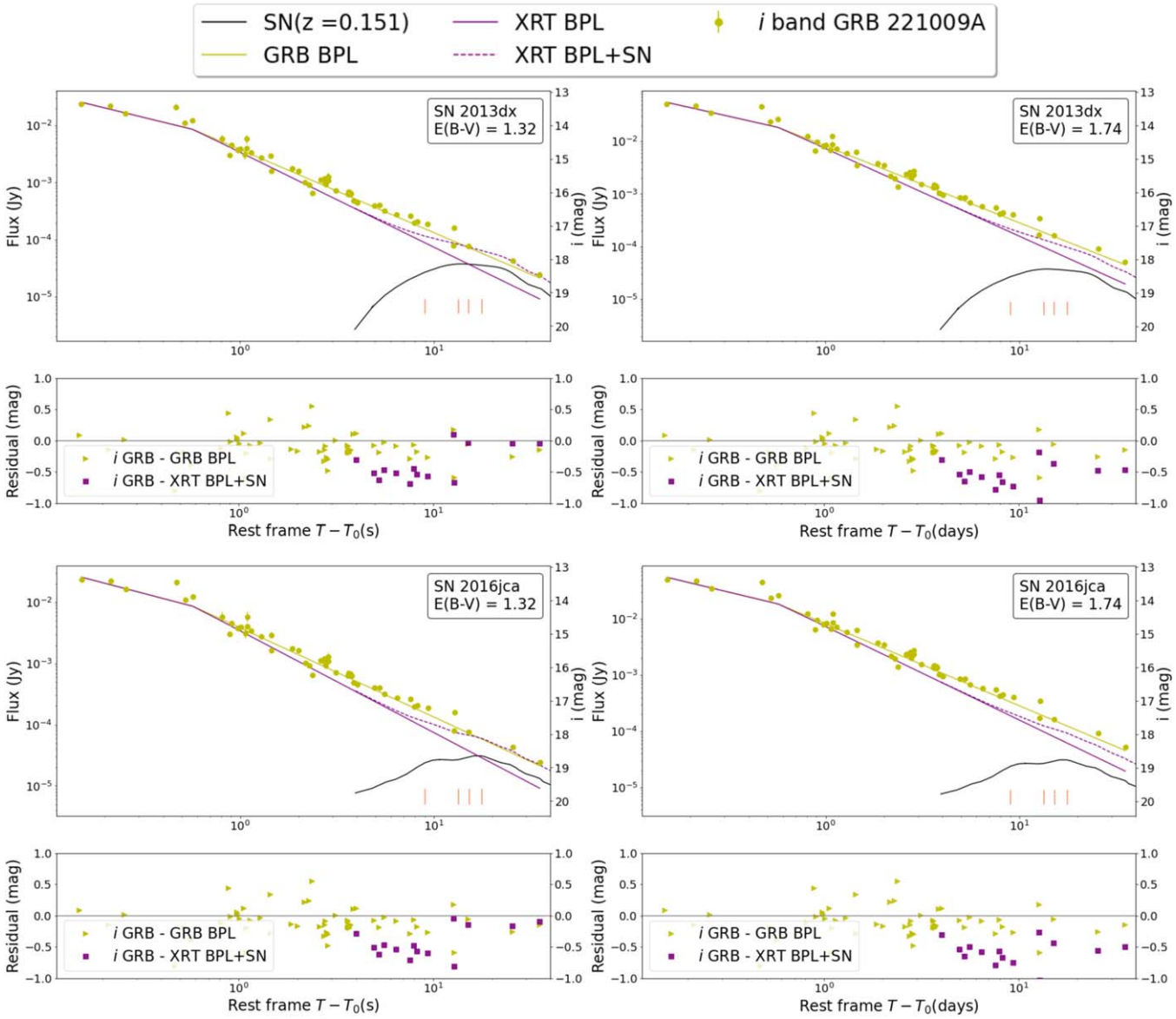

Figure 4. Same plot as Figure 3 for *i* filter. The yellow triangles are the difference between the observed GRB magnitude and broken power-law estimate. The residual plot shows that the broken power-law fit to the GRB optical data is the best fit for the observed data.

(2022); we take this as tentative confirmation of the host redshift.

We also attempted to isolate the SN features in these spectra by modeling the contribution of the GRB afterglow in the spectra. To model the GRB afterglow contribution, we used the analytic function $F_\nu \propto t^{-\alpha}\ \nu^{-\beta}$, where F_ν is the flux, ν is the frequency, β is the spectral index, t is the time since trigger, and α is the photometric decay index. We used our data in the *r*, *i*, and *z* filters from day 6.4 and $E(B-V) = 1.32$ to fit a power law and calculate the spectral decay index. We found $\beta_{\rm opt} = 0.59 \pm 0.17$, which we then used to calculate the flux. We note that our calculated spectral index does not follow $\beta_X = \beta_{\rm opt} + 0.5$, where $\beta_X = 0.9$ is the spectral index from XRT data. We calculated F_ν for the times of each observed spectrum, and we performed photometric calibration to extinction-corrected ($E(B-V) = 1.32$ mag and $E(B-V) = 1.74$ mag) broadband photometry. Finally, we subtracted this contribution from the original spectra to extract SN features. We do not detect any clear SN features such as a broad absorption feature of Si II λ6355 even after this correction in our spectra.

We also compared the spectra of GRB 221009A to two different SNe, SN 1998bw (Patat et al. 2001) and SN 2006aj, associated with GRB 980425 and GRB 060218 (Modjaz et al. 2006; Pian et al. 2006), respectively. We selected these two cases because SN 1998bw is a bright SN associated with GRB, whereas SN 2006aj falls in the lower-luminosity category. We obtained their spectra from the Weizmann Interactive Supernova Data Repository (WISeREP; Yaron & Gal-Yam 2012) at similar phases to our spectra. The SN 1998bw spectra in WISeREP were from Patat et al. (2001), and those for SN 2006aj were from Modjaz et al. (2006) and Pian et al. (2006). These spectra from the archive were first corrected for the Galactic extinction $E(B-V)$ of 0.0509 mag and 0.1253 mag for SN 1998bw and SN 2006aj, respectively. We also shifted the spectra from the redshifts of 0.0085 and 0.0331 for the two SNe to the redshift of GRB 221009A of 0.151. Finally, these redshifted spectra were scaled to match to extinction-

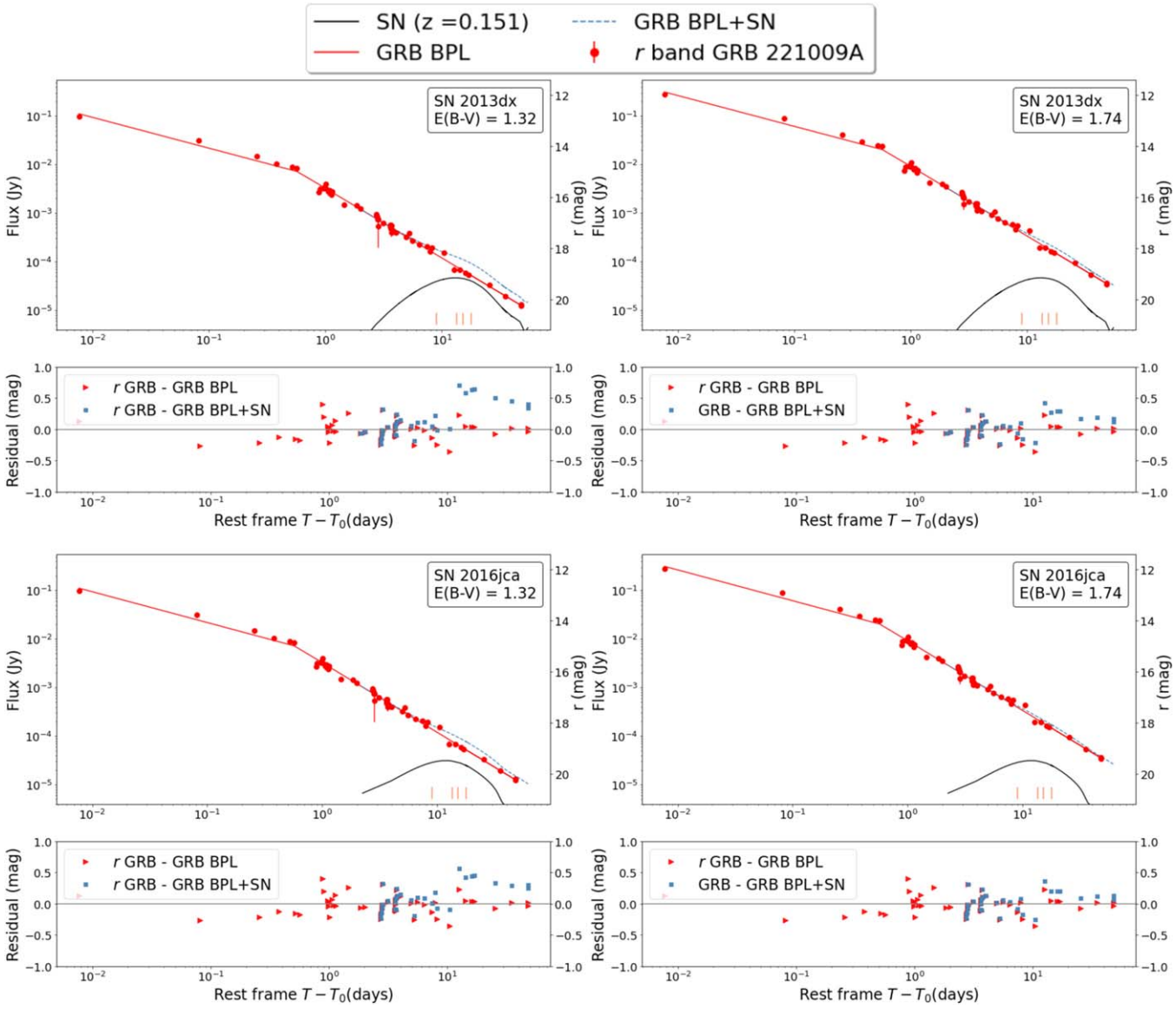

Figure 5. Light curves for the r filter using the two different extinction values of $E(B-V) = 1.32$ mag (left column) and $E(B-V) = 1.74$ mag (right column). SN 2013dx and SN 2016jca light curves are plotted as black solid lines in top and bottom rows, respectively. The sum of SN contribution and GRB afterglow is shown as dashed blue lines. For each case, a residual plot in magnitude is presented. The blue squares are the difference between the SN contribution plus GRB afterglow estimated by a broken power-law fit to the optical data. The red triangles are the difference between the observed GRB magnitude and the broken power-law estimate.

corrected photometry of GRB 221009A. The comparison between the calibrated spectra and the spectra of GRB 221009A at four different epochs is presented in Figure 8. For both the SN 1998bw and SN 2006aj spectra, broad features indicative of SN Ic-BL type can be seen for all the epochs. However, the GRB 221009A spectra are noisier than the SN 1998bw and SN 2006aj spectra. At the first epoch, i.e., 10.40 days after the GRB trigger, our HET spectrum when corrected for $E(B-V) = 1.74$ (blue line in Figure 8) has a similar structure as the other two SNe. However, there are no distinct broad absorption features as expected for SN Ic-BL. MMT spectra at 15.48 days and 17.79 days after the trigger do not show any clear features. For the last spectrum at 20.47 days after the trigger observed by MMT, there is a broad feature with some noise between 6000 and 6500 Å similar to the other two SNe. However, we do not see clear broad absorption features that are indicative of the SN component. We also note that Fulton et al. (2023) reported that the peak of the SN they find associated with the GRB 221009A is 20 days after the trigger, the same as the epoch of our last spectral observation.

4. Discussions and Conclusion

For this work, we observed the location of GRB 221009A both using imaging and spectroscopy to search for SN signatures. We made our first observations using the LBT MODS imager starting 2.5 days after the BAT trigger and augmented our photometry with publicly available data from GCN and HST to do our photometric analysis. Our light-curve modeling does not find an SN bump in the light curve, as would be expected for a GRB with an SN component though we are unable to exclude the presence of a faint SN for a high-extinction case. In addition, we obtained spectroscopic observations from the HET and MMT. The spectra do not contain clear, broad line features indicating associated SN Ic-BL. We summarize the results below:

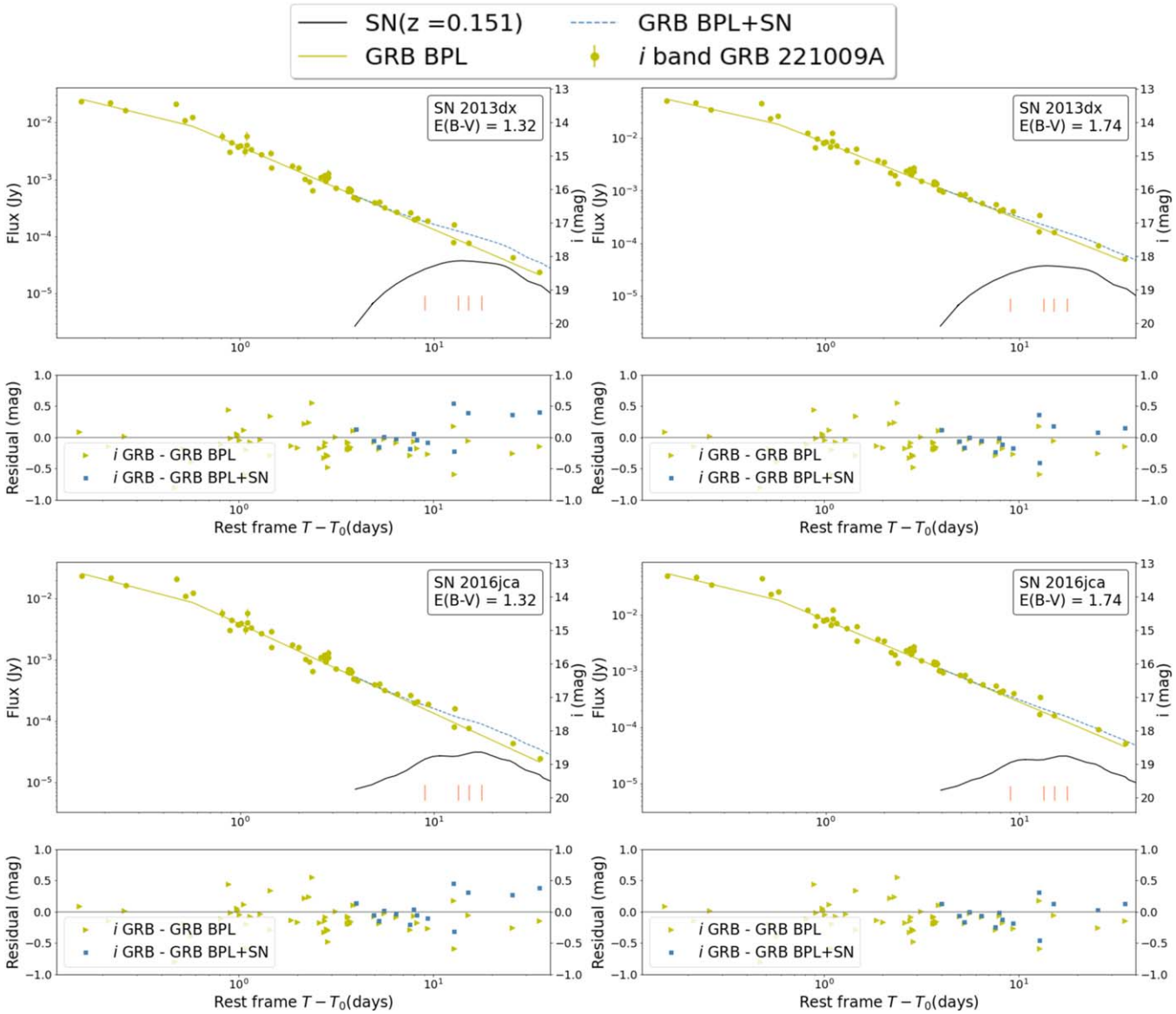

Figure 6. Same plot as Figure 5 for the *i* filter. The blue squares are the difference between SN contribution plus GRB afterglow estimated by broken power law fitted to optical data. The yellow triangles are the difference between the observed GRB magnitude and the broken power-law estimate.

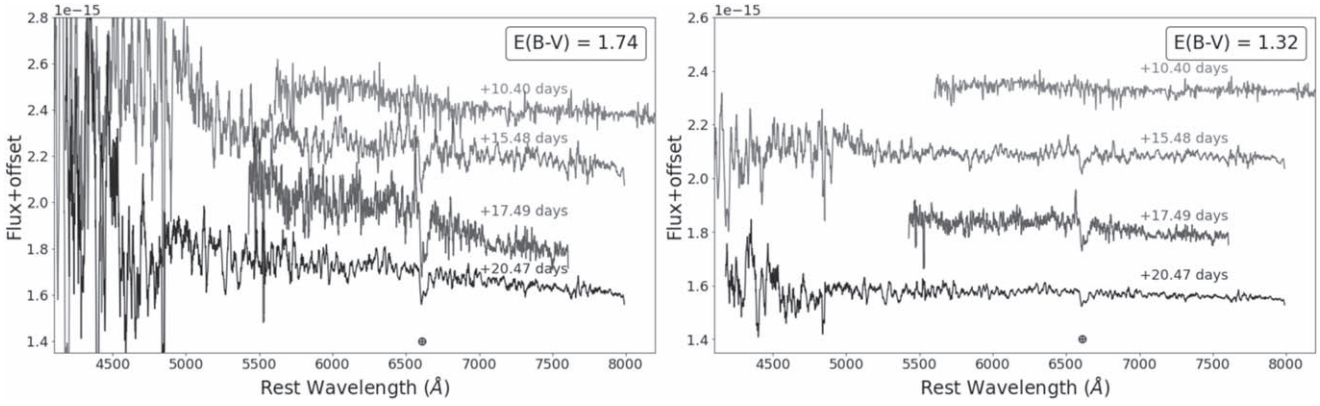

Figure 7. Smoothed spectra of GRB 221009A observed at four different phases of +10.4 (HET), +15.48 (MMT), +17.49 (MMT), and +20.47 (MMT) days after the trigger using two different extinction values of $E(B - V) = 1.32$ mag (left) and $E(B - V) = 1.74$ mag (right). GRB afterglow contributions have been subtracted from the presented spectra. The wavelengths have been converted to the rest frame assuming a redshift of 0.151. No clear SN Ic-BL features are seen in the spectra.

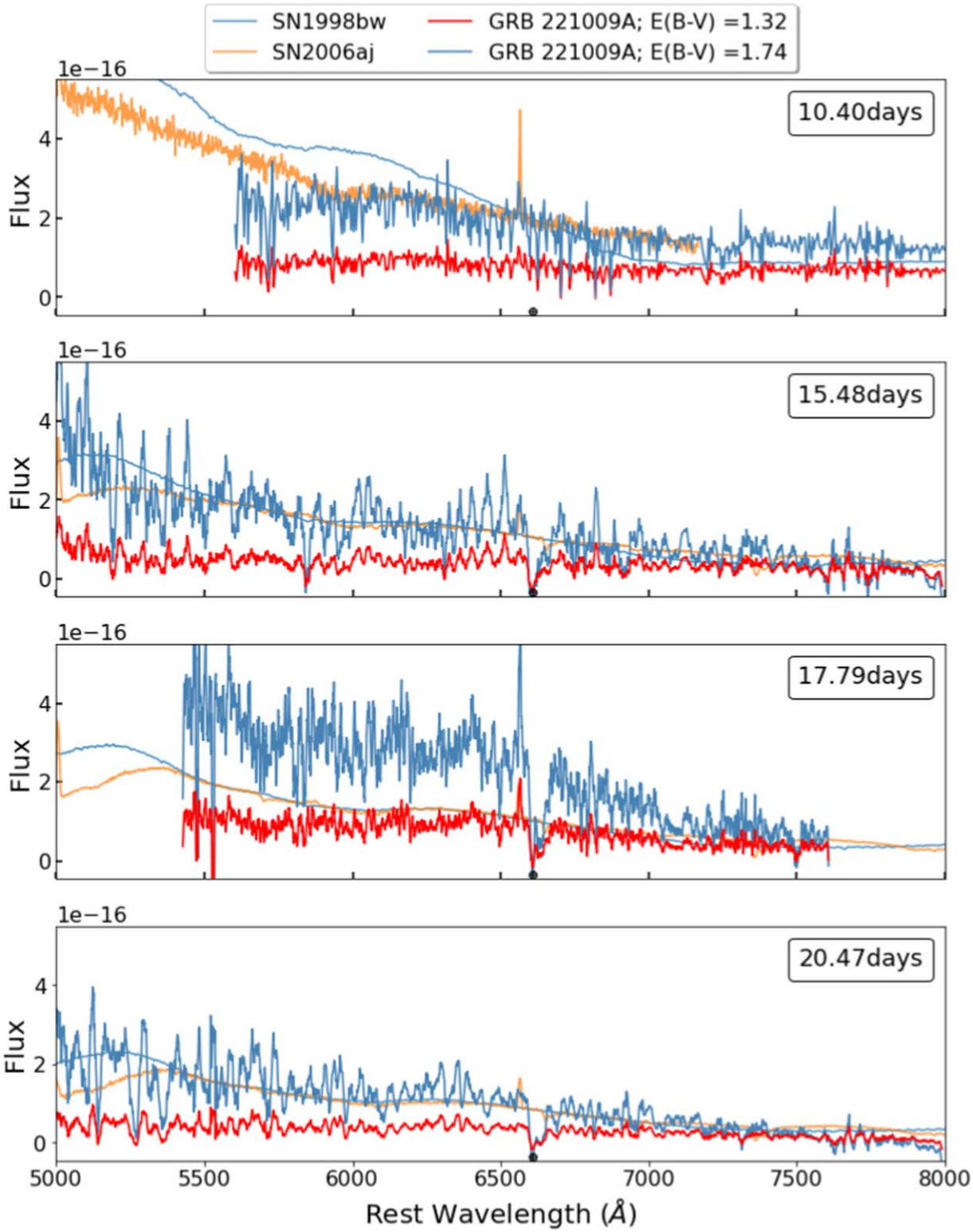

Figure 8. Smoothed spectra of GRB 221009A compared to two SNe, SN 1998bw and SN 2006aj, which were both associated with GRBs. The spectra have been corrected for extinction using the two values used throughout this work ($E(B-V) = 1.32$ mag and $E(B-V) = 1.74$ mag) and have been corrected for their redshift appropriately. All the spectra are calibrated to the photometry of GRB 221009A at the same phase, and the GRB afterglow contribution is subtracted. The four panels are for four different times since the GRB trigger time: 10.40 days, 15.48 days, 17.49 days, and 20.47 days. The spectrum of GRB 221009A at 10.40 days is from HET, and the spectra at 15.48 days, 17.49 days, and 20.47 days are from the MMT. Although the initial HET spectrum bears some resemblance to SN 1998bw in the high-extinction scenario, overall there are no clear SN features present.

1. We investigate if the optical light curves contain contributions from the GRB afterglow and a possible SN. We fit the light curves with two different models. The first model fixes the afterglow contribution to a broken power law with the same decay rate as the X-ray light curve (assumed to be dominated by the GRB

afterglow at all times). The second model is a broken power law with a decay rate fit to match the observed data, which assumes that all of the emission is contributed by the GRB afterglow. We also added an SN component at late times for both cases to check if the observed light curve could be the result of afterglow and SN emission for the first model and if an SN component would have been identified for the second model.

2. We checked how the light curve would evolve in the presence of two different SNe at a similar redshift to GRB 221009A. In all cases, we find that the afterglow+SN model provides a worse fit to the data than the afterglow-only model. Thus, we do not find evidence of a bright SN in our light curve.
3. We observed the spectrum of GRB 221009A to search for spectroscopic signatures of an SN. We modeled the GRB afterglow contribution to the spectrum as $F_\nu \propto t^{-\alpha} \nu^{-\beta}$. We estimated the value of β using optical photometry. Subtraction of this contribution does not change the features of the spectra. It only brings the flux values closer to zero. We do not detect any consistent, broad features across our spectroscopic sequence. Hence, no clear SN contribution is detected.

Our study shows that we do not detect an SN associated with GRB 221009A. However, we cannot discard the possibility that there could be an associated SN below our detection limit if we consider the high extinction. The lack of SN features could be due to the SN being fainter than SN 2013dx or SN 2016jca (i.e., with an absolute magnitude of $M_r > -19.5$ and $M_i > -19.3$) or due to the high extinction in the direction of GRB 221009A, which could hide the SN features. Our nondetection of an SN from GRB 221009A at this level may suggest that most of the energy produced by the central engine is carried by the relativistic jet, not the bulk ejecta.

We also consider our results in the context of the small but growing sample of GRBs detected at very high gamma-ray energies (TeV). In the case of GRB 190114C, the first GRB with associated TeV photons, an associated SN was also seen (SN 2019jrj; Melandri et al. 2022). Interestingly, the spectral analysis of Melandri et al. (2022) shows that SN 2019jrj's absorption lines are more similar to those of less luminous CCSNe such as SNe 2004aw (Taubenberger et al. 2006) or 2002ap (Tomita et al. 2006) than to other GRB-SNe. Specifically, SN 2019jrj's emission lines are narrower, meaning that its ejecta was more slowly moving and carried less energy. The photometric analysis of Melandri et al. (2022) shows that the luminosity of SN 2019jrj is lower than SN 2013dx. This luminosity range would be below our detection limit if we assume the extinction to be 1.74 mag for GRB 221009A. In this case, our results suggest the possibility that GRBs capable of accelerating photons to TeV energies are accompanied by underluminous SNe, possibly providing clues to their central engines and progenitors.

Fulton et al. (2023) reported the detection of an SN component in their optical light curve of GRB 221009A obtained mainly with Pan-STARRS and a few other telescopes. They assume the X-ray decay index as the GRB afterglow decay index and find excess flux in the r, i, and y filters and not in the z filter. They find the excess flux follows a similar behavior to SN 2016jca and SN 2017iuk. Thus, this excess is explained as an emerging SN with absolute peak AB magnitudes of $M_g = -19.8 \pm 0.6$ mag, $M_r = -19.5 \pm 0.3$, and $M_z = -20.1 \pm 0.3$. Since we do not have good coverage in the z-band light curve, and we did not collect any y band, we have not included these bands in our analyses, whereas, for the r and i filters, we have good coverage of the data set and have done a similar analysis. For our data set, we also find excess in flux when compared to a power law based on the X-ray data. However, our analyses show that this excess is better explained by a simple broken power-law fit to optical data rather than the addition of a bright SN component with $M_r = -19.5$ mag. The shallowness in the optical decay can be explained by the relation $\alpha_X = \alpha_{\rm opt} + 0.25$ expected for the slow cooling regime for constant interstellar medium (Zaninoni et al. 2013). If we assume the observed data to be explained by a broken power law with a decay index shallower than the XRT data, and also $E(B-V) = 1.74$ mag, in that case, there could be an associated SN with $M_r = -19.5$ mag, which would not show a clear bump in the r-band light curve.

We note that de Ugarte Postigo et al. (2022a) and Rossi et al. (2022a) reported via GCN circulars the detection of associated SN spectroscopically at an average time of 8 and 8.56 days after the BAT trigger. From our light-curve analysis, for us to detect SN bumps during that time period, the absolute magnitude of the associated SN would have to be brighter than $M_r = -20.66$ after correcting for the extinction of $E(B-V) = 1.32$ mag. This value is greater than the absolute magnitude at the peak for both SN 1998bw ($M_r = -19.41$) and SN 2012bz ($M_r = -19.63$). We also note that our MMT spectra at the last epoch coincide with the predicted peak in the SN component from the analyses of Fulton et al. (2023). However, we do not see any broad features in our spectrum (Figure 7) that is indicative of SN type Ic-BL. We note that our spectrum is noisy compared to other SN spectra as shown in Figure 8 for comparison.

Alternately, our results could indicate that GRB 221009A has no associated SN at all. Previously, there have been observations of SN-less GRBs such as GRB 060505 (Fynbo et al. 2006), GRB 060614 (Della Valle et al. 2006; Fynbo et al. 2006; Gal-Yam et al. 2006), GRB 111005A (MichałowskI et al. 2018), and GRB 2211211A (Rastinejad et al. 2022). For all of these cases, unlike GRB 221009A, the source is not located in a region of high extinction. Thus, dust extinction has been ruled out for the three SN-less GRBs. For the case of GRB 060614, the afterglow is faint, and even an SN similar to SN 2006aj would be clearly visible in the light curve, ruling out the possibility of even a very faint associated SN. Dado & Dar (2018) suggest that such SN-less GRBs could comprise half of the GRB population and could originate from a phase transition of neutron stars to quark stars in high-mass X-ray binaries.

Recently, the bright GRB 211211A with redshift ($z = 0.0763 \pm 0.0002$) was also found to have no associated SN (Rastinejad et al. 2022; Troja et al. 2022). Instead, its light curve shows an excess in the NIR, which points toward an associated kilonova and a binary neutron star merger origin. In the case of GRB 221009A, we do not detect a strong infrared excess indicative of an associated kilonova and thus consider a compact object merger scenario unlikely for this burst. Long-term monitoring of GRB 221009A, including with powerful facilities like HST and JWST, will improve our understanding of the afterglow model and improve our limits on a possible SN contribution, providing new tests of these and other models for the progenitors and central engines powering the most energetic GRBs.

We are grateful to J. Rastinejad & W.-F. Fong for help with the MMT observing and comments on an earlier version of the manuscript. We also thank B. Weiner for help with the MMT observations. We would also like to thank our anonymous referee for constructive comments on the paper, which have greatly improved the paper. We also like to thank E. Pian for sharing SN 2013dx and SN 2106jca light-curve data.

Time domain research by the University of Arizona team and D.J.S. is supported by NSF grants AST-1821987, 1813466, 1908972, & 2108032, and by the Heising-Simons Foundation under grant #20201864.

This publication was made possible through the support of an LSSTC Catalyst Fellowship to K.A.B., funded through grant 62192 from the John Templeton Foundation to LSST Corporation. The opinions expressed in this publication are those of the authors and do not necessarily reflect the views of LSSTC or the John Templeton Foundation.

Observations reported here were obtained at the MMT Observatory, a joint facility of the University of Arizona and the Smithsonian Institution. This paper uses data taken with the MODS spectrographs built with funding from NSF grant AST-9987045 and the NSF Telescope System Instrumentation Program (TSIP), with additional funds from the Ohio Board of Regents and the Ohio State University Office of Research.

This research has made use of the NASA Astrophysics Data System (ADS) Bibliographic Services, and the NASA/IPAC Infrared Science Archive (IRSA), which is funded by the National Aeronautics and Space Administration and operated by the California Institute of Technology. This research made use of Photutils, an Astropy package for detection and photometry of astronomical sources (Bradley et al. 2019).

This work made use of data supplied by the UK Swift Science Data Centre at the University of Leicester. The DELVE project is partially supported by the NASA Fermi Guest Investigator Program Cycle 9 No. 91201. This manuscript has been authored by Fermi Research Alliance, LLC under Contract No. DE-AC02-07CH11359 with the U.S. Department of Energy, Office of Science, Office of High Energy Physics. The United States Government retains and the publisher, by accepting the article for publication, acknowledges that the United States Government retains a non-exclusive, paid-up, irrevocable, world wide license to publish or reproduce the published form of this manuscript or allow others to do so, for United States Government purposes. This project used data obtained with the Dark Energy Camera (DECam), which was constructed by the Dark Energy Survey (DES) collaboration. Funding for the DES Projects has been provided by the US Department of Energy, the US National Science Foundation, the Ministry of Science and Education of Spain, the Science and Technology Facilities Council of the United Kingdom, the Higher Education Funding Council for England, the National Center for Supercomputing Applications at the University of Illinois at Urbana-Champaign, the Kavli Institute for Cosmological Physics at the University of Chicago, Center for Cosmology and Astro-Particle Physics at the Ohio State University, the Mitchell Institute for Fundamental Physics and Astronomy at Texas A&M University, Financiadora de Estudos e Projetos, Fundação Carlos Chagas Filho de Amparo à Pesquisa do Estado do Rio de Janeiro, Conselho Nacional de Desenvolvimento Científico e Tecnológico and the Ministério da Ciência, Tecnologia e Inovação, the Deutsche Forschungsgemeinschaft and the Collaborating Institutions in the Dark Energy Survey. The Collaborating Institutions are Argonne National Laboratory, the University of California at Santa Cruz, the University of Cambridge, Centro de Investigaciones Enérgeticas, Medioambientales y Tecnológicas-Madrid, the University of Chicago, University College London, the DES-Brazil Consortium, the University of Edinburgh, the Eidgenössische Technische Hochschule (ETH) Zürich, Fermi National Accelerator Laboratory, the University of Illinois at Urbana-Champaign, the Institut de Ciències de l'Espai (IEEC/CSIC), the Institut de Física d'Altes Energies, Lawrence Berkeley National Laboratory, the Ludwig-Maximilians Universität München and the associated Excellence Cluster Universe, the University of Michigan, NSF's NOIRLab, the University of Nottingham, the Ohio State University, the OzDES Membership Consortium, the University of Pennsylvania, the University of Portsmouth, SLAC National Accelerator Laboratory, Stanford University, the University of Sussex, and Texas A&M University.

Based on observations at Cerro Tololo Inter-American Observatory, NSF's NOIRLab (NOIRLab Prop. ID 2022B-827437; PI: G. Hosseinzadeh; 2019A-0305; PI: A. Drlica-Wagner), which is managed by the Association of Universities for Research in Astronomy (AURA) under a cooperative agreement with the National Science Foundation.

Based in part on observations obtained at the Southern Astrophysical Research (SOAR) telescope, which is a joint project of the Ministério da Ciência, Tecnologia e Inovações (MCTI/LNA) do Brasil, the US National Science Foundation's NOIRLab, the University of North Carolina at Chapel Hill (UNC), and Michigan State University (MSU). The observations reported here were obtained in part at the MMT Observatory, a facility operated jointly by the Smithsonian Institution and the University of Arizona. MMT telescope time was granted by NSF's NOIRLab, through the Telescope System Instrumentation Program (TSIP). TSIP was funded by NSF (NOIRLab Prop. ID UAO-S143-22B ; PI: S. Wyatt).

This research is based on observations made with the NASA/ESA Hubble Space Telescope obtained from the Space Telescope Science Institute, which is operated by the Association of Universities for Research in Astronomy, Inc., under NASA contract NAS 5-26555. These observations are associated with program 17264. The authors acknowledge the team led by PI A. J. Levan for developing their observing program with a zero-exclusive-access period.

The Low Resolution Spectrograph 2 (LRS2) was developed and funded by the University of Texas at Austin McDonald Observatory and Department of Astronomy, and by Pennsylvania State University. We thank the Leibniz-Institut fur Astrophysik Potsdam (AIP) and the Institut fur Astrophysik Goettingen (IAG) for their contributions to the construction of the integral field units. Based on observations obtained with the Hobby–Eberly Telescope (HET), which is a joint project of the University of Texas at Austin, the Pennsylvania State University, Ludwig-Maximillians-Universitaet Muenchen, and Georg-August Universitaet Goettingen. The HET is named in honor of its principal benefactors, William P. Hobby and Robert E. Eberly.

This research has made use of the CfA Supernova Archive, which is funded in part by the National Science Foundation through grant AST 0907903. This work makes use of data taken with the Las Cumbres Observatory global telescope

network. The LCO group is supported by NSF grants 1911225 and 1911151.

J.E.A. and C.E.M.V. are supported by the international Gemini Observatory, a program of NSF's NOIRLab, which is managed by the Association of Universities for Research in Astronomy (AURA) under a cooperative agreement with the National Science Foundation, on behalf of the Gemini partnership of Argentina, Brazil, Canada, Chile, the Republic of Korea, and the United States of America. J.A.C.-B. acknowledges support from FONDECYT Regular No. 1220083.

Facilities: ADS, CTIO:DECam, LBT (MODS), MMT (Binospec), HET (LRS2), Las Cumbres Observatory (MUSCAT3), NED, SOAR (GHTS), WISeREP, HST, IRSA.

Software: astropy (Astropy Collaboration et al. 2013; Price-Whelan et al. 2018), Photutils (Bradley et al. 2019), Binospec IDL (Kansky et al. 2019), Panacea, BANZAI (McCully et al. 2018), Light Curve Fitting (Hosseinzadeh & Gomez 2020), MatPLOTLIB (Hunter 2007), NumPy (Harris et al. 2020), Scipy (Virtanen et al. 2020), IRAF (Tody 1986, 1993).

ORCID iDs

Manisha Shrestha https://orcid.org/0000-0002-4022-1874
David J. Sand https://orcid.org/0000-0003-4102-380X
Kate D. Alexander https://orcid.org/0000-0002-8297-2473
K. Azalee Bostroem https://orcid.org/0000-0002-4924-444X
Griffin Hosseinzadeh https://orcid.org/0000-0002-0832-2974
Jeniveve Pearson https://orcid.org/0000-0002-0744-0047
Mojgan Aghakhanloo https://orcid.org/0000-0001-8341-3940
József Vinkó https://orcid.org/0000-0001-8764-7832
Jennifer E. Andrews https://orcid.org/0000-0003-0123-0062
Jacob E. Jencson https://orcid.org/0000-0001-5754-4007
M. J. Lundquist https://orcid.org/0000-0001-9589-3793
Samuel Wyatt https://orcid.org/0000-0003-2732-4956
D. Andrew Howell https://orcid.org/0000-0003-4253-656X
Curtis McCully https://orcid.org/0000-0001-5807-7893
Estefania Padilla Gonzalez https://orcid.org/0000-0003-0209-9246
Craig Pellegrino https://orcid.org/0000-0002-7472-1279
Giacomo Terreran https://orcid.org/0000-0003-0794-5982
Daichi Hiramatsu https://orcid.org/0000-0002-1125-9187
Joseph Farah https://orcid.org/0000-0003-4914-5625
Saurabh W. Jha https://orcid.org/0000-0001-8738-6011
Nathan Smith https://orcid.org/0000-0001-5510-2424
J. Craig Wheeler https://orcid.org/0000-0003-1349-6538
Clara Martínez-Vázquez https://orcid.org/0000-0002-9144-7726
Julio A. Carballo-Bello https://orcid.org/0000-0002-3690-105X
Alex Drlica-Wagner https://orcid.org/0000-0001-8251-933X
David J. James https://orcid.org/0000-0001-5160-4486
Burçin Mutlu-Pakdil https://orcid.org/0000-0001-9649-4815
Guy S. Stringfellow https://orcid.org/0000-0003-1479-3059
Joanna D. Sakowska https://orcid.org/0000-0002-1594-1466
Noelia E. D. Noël https://orcid.org/0000-0002-8282-469X
Clécio R. Bom https://orcid.org/0000-0003-4383-2969
Kyler Kuehn https://orcid.org/0000-0003-0120-0808

References

Ashall, C., Mazzali, P. A., Pian, E., et al. 2019, MNRAS, 487, 5824
Astropy Collaboration, Robitaille, T. P., Tollerud, E. J., et al. 2013, A&A, 558, A33
Atteia, J. L. 2022, GCN, 32793, 1
Balaji, S., Ramirez-Quezada, M. E., Silk, J., & Zhang, Y. 2023, arXiv:2301.02258
Barbary, K. 2016, extinction v0.3.0, Zenodo, doi:10.5281/zenodo.804967
Belkin, S., Kim, V., Pozanenko, A., et al. 2022a, GCN, 32769, 1
Belkin, S., Nazarov, S., Pozanenko, A., Pankov, N. & IKI GRB FuN 2022b, GCN, 32684, 1
Belkin, S., Pozanenko, A., Klunko, E., Pankov, N. & GRB IKI FuN 2022c, GCN, 32645, 1
Bennett, C. L., Larson, D., Weiland, J. L., & Hinshaw, G. 2014, ApJ, 794, 135
Bikmaev, I., Khamitov, I., Irtuganov, E., et al. 2022a, GCN, 32743, 1
Bikmaev, I., Khamitov, I., Irtuganov, E., et al. 2022b, GCN, 32752, 1
Bradley, L., Sipőcz, B., Robitaille, T., et al. 2019, astropy/photutils: v0.6, doi:10.5281/zenodo.2533376
Brivio, R., Ferro, M., D'Avanzo, P., et al. 2022, GCN, 32652, 1
Brown, T. M., Baliber, N., Bianco, F. B., et al. 2013, PASP, 125, 1031
Butler, N., Watson, A. M., Dichiara, S., et al. 2022, GCN, 32705, 1
Cano, Z., Izzo, L., de Ugarte Postigo, A., et al. 2017b, A&A, 605, A107
Cano, Z., Wang, S.-Q., Dai, Z.-G., & Wu, X.-F. 2017a, AdAst, 2017, 8929054
Castro-Tirado, A. J., Sanchez-Ramirez, R., Hu, Y. D., et al. 2022, GCN, 32686, 1
Chambers, K. C., Magnier, E. A., Metcalfe, N., et al. 2016, arXiv:1612.05560
Chen, T. W., Malesani, D. B., Yang, S., et al. 2022, GCN, 32667, 1
Clemens, J. C., Crain, J. A., & Anderson, R. 2004, Proc. SPIE, 5492, 331
Dado, S., & Dar, A. 2018, ApJ, 855, 88
Dainotti, M. G., Simone, B. D., Islam, K. M., et al. 2022, ApJ, 938, 41
D'Avanzo, P., Ferro, M., Brivio, R., et al. 2022, GCN, 32755, 1
de Ugarte Postigo, A., Izzo, L., Pugliese, G., et al. 2022b, GCN, 32648, 1
de Ugarte Postigo, A., Izzo, L., Thoene, C. C., et al. 2022a, GCN, 32800, 1
de Wet, S., Groot, P. J. & Meerlicht Consortium 2022, GCN, 32646, 1
Della Valle, M., Chincarini, G., Panagia, N., et al. 2006, Natur, 444, 1050
Dressel, L. 2022, Wide Field Camera 3, HST Instrument Handbook (Baltimore, MD: Space Telescope Science Institute), 14
Drlica-Wagner, A., Carlin, J. L., Nidever, D. L., et al. 2021, ApJS, 256, 2
Drlica-Wagner, A., Ferguson, P. S., Adamów, M., et al. 2022, ApJS, 261, 38
Drout, M. R., Soderberg, A. M., Gal-Yam, A., et al. 2011, ApJ, 741, 97
Dzhappuev, D. D., Afashokov, Y. Z., Dzaparova, I. M., et al. 2022, ATel, 15669, 1
Evans, C. J., Simard, L., Takami, H., et al. 2016, Proc. SPIE, 9908, 99084C
Evans, P. A., Beardmore, A. P., Page, K. L., et al. 2009, MNRAS, 397, 1177
Fabricant, D., Fata, R., Epps, H., et al. 2019a, PASP , 131, 075004
Ferro, M., Brivio, R., D'Avanzo, P., et al. 2022, GCN, 32804, 1
Filippenko, A. V. 1997, ARA&A, 35, 309
Flaugher, B., Diehl, H. T., Honscheid, K., et al. 2015, AJ, 150, 150
Fulton, M. D., Smartt, S. J., Rhodes, L., et al. 2023, arXiv:2301.11170
Fynbo, J. P. U., Watson, D., Thöne, C. C., et al. 2006, Natur, 444, 1047
Galama, T. J., Vreeswijk, P. M., van Paradijs, J., et al. 1998, Natur, 395, 670
Gal-Yam, A., Fox, D. B., Price, P. A., et al. 2006, Natur, 444, 1053
Gaskell, C. M., Cappellaro, E., Dinerstein, H. L., et al. 1986, ApJL, 306, L77
Groot, P. J., Vreeswijk, P. M., Ter Horst, R., et al. 2022, GCN, 32678, 1
Harris, C. R., Millman, K. J., van der Walt, S. J., et al. 2020, Natur, 585, 357
Hill, G. J., Lee, H., MacQueen, P. J., et al. 2021, AJ, 162, 298
Hjorth, J., & Bloom, J. S. 2012, in Gamma-Ray Bursts, ed. C. Kouveliotou, R. A. M. J. Wijers, & S. Woosley (Cambridge: Cambridge Univ. Press), 169
Hosseinzadeh, G., & Gomez, S. 2020, Light Curve Fitting, v0.2.0, Zenodo, doi:10.5281/zenodo.4312178
Hosseinzadeh, G., & Gomez, S. 2022, Light Curve Fitting, v0.7.0, Zenodo, doi:10.5281/zenodo.7250571
Hu, Y. D., Casanova, V., Fernandez-Garcia, E., et al. 2022, GCN, 32644, 1
Huang, Y., Hu, S., Chen, S., et al. 2022, GCN, 32677, 1
Huber, M., Schultz, A., Chambers, K. C., et al. 2022, GCN, 32758, 1
Hunter, J. D. 2007, CSE, 9, 90
Iwamoto, K., Mazzali, P. A., Nomoto, K., et al. 1998, Natur, 395, 672
Izzo, L., Saccardi, A., Fynbo, J. P. U., et al. 2022, GCN, 32765, 1
Kann, D. A., Agayeva, S., Aivazyan, V., et al. 2023, arXiv:2302.06225
Kansky, J., Chilingarian, I., Fabricant, D., et al. 2019, PASP, 131, 075005
Kass, R. E., & Raftery, A. E. 1995, JASA, 90, 773
Kim, V., Krugov, M., Pozanenko, A., et al. 2022, GCN, 32670, 1
Kimura, M., Isogai, K., Arimoto, M., et al. 2022, GCN, 33038, 1
Kulkarni, S. R., Frail, D. A., Wieringa, M. H., et al. 1998, Natur, 395, 663
Kumar, H., Swain, V., Waratkar, G., et al. 2022, GCN, 32662, 1
Laskar, T., Alexander, K. D., Ayache, E., et al. 2022, GCN, 32757, 1
Laskar, T., Alexander, K. D., Margutti, R., et al. 2023, ApJL, submitted arXiv:2302.04388
Levan, A. J., Barclay, T., Bhirombhakdi, K., et al. 2022, GCN, 32921, 1
Levan, A. J., Lamb, G. P., Schneider, B., et al. 2023, arXiv:2302.07761
MAGIC Collaboration, Acciari, V. A., Ansoldi, S., et al. 2019, Natur, 575, 455
Mao, J., Lu, K. X., Zhao, X. H., & Bai, J. M. 2022, GCN, 32727, 1

Mazzali, P. A., Pian, E., Bufano, F., & Ashall, C. 2021, MNRAS, 505, 4106
McCully, C., Volgenau, N. H., Harbeck, D.-R., et al. 2018, Proc. SPIE, 10707, 107070K
Melandri, A., Izzo, L., Pian, E., et al. 2022, A&A, 659, A39
MichałowskI, M. J., Xu, D., Stevens, J., et al. 2018, A&A, 616, A169
Mirabal, N. 2023, MNRAS, 519, L85
Modjaz, M., Bianco, F. B., Siwek, M., et al. 2020, ApJ, 892, 153
Modjaz, M., Kewley, L., Bloom, J. S., et al. 2011, ApJL, 731, L4
Modjaz, M., Liu, Y. Q., Bianco, F. B., & Graur, O. 2016, ApJ, 832, 108
Modjaz, M., Stanek, K. Z., Garnavich, P. M., et al. 2006, ApJL, 645, L21
Narita, N., Fukui, A., Yamamuro, T., et al. 2020, Proc. SPIE, 11447, 114475K
Nomoto, K., Iwamoto, K., & Suzuki, T. 1995, PhR, 256, 173
O'Connor, B., Cenko, S. B., Troja, E., et al. 2022a, GCN, 32739, 1
O'Connor, B., Cenko, S. B., Troja, E., et al. 2022b, GCN, 32799, 1
O'Connor, B., Troja, E., Dichiara, S., Gillanders, J., & Cenko, S. B. 2022c, GCN, 32750, 1
O'Connor, B., Troja, E., Dichiara, S., Gillanders, J., & Cenko, S. B. 2022d, GCN, 32860, 1
Paek, G. S. H., Im, M., Urata, Y., & Sung, H.-I. 2022, GCN, 32659, 1
Patat, F., Cappellaro, E., Danziger, J., et al. 2001, ApJ, 555, 900
Perley, D. A. 2022, GCN, 32638, 1
Pian, E., Mazzali, P. A., Masetti, N., et al. 2006, Natur, 442, 1011
Podsiadlowski, P., Hsu, J. J. L., Joss, P. C., & Ross, R. R. 1993, Natur, 364, 509
Pogge, R. W., McLean, I. S., Ramsay, S. K., et al. 2010, Proc. SPIE, 7735, 77350A
Popowski, P., Cook, K. H., & Becker, A. C. 2003, AJ, 126, 2910
Price-Whelan, A. M., Sipőcz, B. M., Günther, H. M., et al. 2018, AJ, 156, 123
Rajabov, Y., Sadibekova, T., Tillayev, Y., et al. 2022, GCN, 32795, 1
Ramsey, L. W., Adams, M. T., Barnes, T. G., et al. 1998, Proc. SPIE, 3352, 34
Rastinejad, J., & Fong, W. 2022, GCN, 32749, 1
Rastinejad, J. C., Gompertz, B. P., Levan, A. J., et al. 2022, Natur, 612, 223
Romanov, F. D. 2022a, GCN, 32664, 1
Romanov, F. D. 2022b, GCN, 32679, 1
Rossi, A., Maiorano, E., Malesani, D. B., et al. 2022a, GCN, 32809, 1
Rossi, A., Rothberg, B., Palazzi, E., et al. 2022b, ApJ, 932, 1
Rowles, J., & Froebrich, D. 2009, MNRAS, 395, 1640
Sasada, M., Imai, Y., Murata, K. L., et al. 2022, GCN, 32730, 1
Schlafly, E. F., & Finkbeiner, D. P. 2011, ApJ, 737, 103
Schlegel, D. J., Finkbeiner, D. P., & Davis, M. 1998, ApJ, 500, 525
Schneider, B., Adami, C., Le Floc'h, E., et al. 2022, GCN, 32753, 1
Shetrone, M., Cornell, M., Fowler, J., et al. 2007, PASP, 119, 556
Shresta, M., Sand, D., Alexander, K. D., et al. 2022, GCN, 32759, 1
Shrestha, M., Bostroem, K., Sand, D., et al. 2022, GCN, 32771, 1
Smartt, S. J. 2009, ARA&A, 47, 63
Strausbaugh, R., & Cucchiara, A. 2022a, GCN, 32693, 1
Strausbaugh, R., & Cucchiara, A. 2022b, GCN, 32738, 1
Tanga, M., Krühler, T., Schady, P., et al. 2018, A&A, 615, A136
Taubenberger, S., Pastorello, A., Mazzali, P. A., et al. 2006, MNRAS, 371, 1459
Tody, D. 1986, Proc. SPIE, 627, 733
Tody, D. 1993, ASP Conf. Ser. 52, Astronomical Data Analysis Software and Systems II, 52 ed. R. J. Hanisch, R. J. V. Brissenden, & J. Barnes (San Francisco, CA: ASP), 173
Tomita, H., Deng, J., Maeda, K., et al. 2006, ApJ, 644, 400
Toy, V. L., Cenko, S. B., Silverman, J. M., et al. 2016, ApJ, 818, 79
Troja, E., Fryer, C. L., O'Connor, B., et al. 2022, Natur, 612, 228
Valdes, F., & Gruendl, R. 2014, in ASP Conf. Ser. 485, Astronomical Data Analysis Software and Systems XXIII, ed. N. Manset & P. Forshay (San Francisco, CA: ASP), 379
Veres, P., Burns, E., Bissaldi, E., et al. 2022, GCN, 32636, 1
Vidal, E., Zheng, W., Filippenko, A. V. & KAIT GRB team 2022, GCN, 32669, 1
Vinko, J., Bodi, A., Pal, A., et al. 2022, GCN, 32709, 1
Virtanen, P., Gommers, R., Oliphant, T. E., et al. 2020, NatMe, 17, 261
Woosley, S. E., & Bloom, J. S. 2006, ARA&A, 44, 507
Xu, D., Jiang, S. Q., Fu, S. Y., et al. 2022, GCN, 32647, 1
Yang, Y., Hoeflich, P., Baade, D., et al. 2020, ApJ, 902, 46
Yaron, O., & Gal-Yam, A. 2012, PASP, 124, 668
Zaninoni, E., Bernardini, M. G., Margutti, R., Oates, S., & Chincarini, G. 2013, A&A, 557, A12
Zaznobin, I., Burenin, R., & Eselevich, M. 2022, GCN, 32729, 1